

CO₂ emissions trends in the Los Angeles megacity

S. Newman et al.

Toward consistency between bottom-up CO₂ emissions trends and top-down atmospheric measurements in the Los Angeles megacity

S. Newman¹, X. Xu², K. R. Gurney³, Y.-K. Hsu⁴, K.-F. Li⁵, X. Jiang⁶, R. Keeling⁷, S. Feng^{8,a}, D. O’Keefe³, R. Patarasuk³, K. W. Wong⁸, P. Rao⁸, M. L. Fischer⁹, and Y. L. Yung¹

¹Division of Geological and Planetary Sciences, California Institute of Technology, Pasadena, CA 91125, USA

²Department of Earth System Science, University of California, Irvine, CA 92697, USA

³School of Life Sciences, Arizona State University, Tempe, AZ 85287, USA

⁴Monitoring and Laboratory Division, Air Resources Board, Sacramento, CA 95811, USA

⁵Department of Applied Mathematics, University of Washington, Seattle, WA 98195, USA

⁶Department of Earth and Atmospheric Sciences, University of Houston, Houston, TX 77004, USA

⁷Scripps Institution of Oceanography, University of California, San Diego, La Jolla, CA 92037, USA

Title Page

Abstract

Introduction

Conclusions

References

Tables

Figures



Back

Close

Full Screen / Esc

Printer-friendly Version

Interactive Discussion



⁸Earth Atmospheric Science, Jet Propulsion Laboratory, California Institute of Technology, Pasadena, CA 91109, USA

⁹Environmental Energy Area, E. O. Lawrence Berkeley National Laboratory, Berkeley, CA 94720, USA

^anow at: Department of Meteorology, Pennsylvania State University, University Park, PA 16802, USA

Received: 9 September 2015 – Accepted: 29 September 2015 – Published: 29 October 2015

Correspondence to: S. Newman (sally@gps.caltech.edu)

Published by Copernicus Publications on behalf of the European Geosciences Union.

CO₂ emissions trends in the Los Angeles megacity

S. Newman et al.

Title Page	
Abstract	Introduction
Conclusions	References
Tables	Figures
◀	▶
◀	▶
Back	Close
Full Screen / Esc	
Printer-friendly Version	
Interactive Discussion	



Abstract

Large urban emissions of greenhouse gases result in large atmospheric enhancements relative to background that are easily measured. Using CO₂ mole fractions and $\Delta^{14}\text{C}$ and $\delta^{13}\text{C}$ values of CO₂ in the Los Angeles megacity observed in inland Pasadena (2006–2013) and coastal Palos Verdes peninsula (autumn 2009–2013), we have determined time series for CO₂ contributions from fossil fuel combustion for both sites and broken those down into contributions from petroleum/gasoline and natural gas burning for Pasadena. We find a 10% reduction in Pasadena CO₂ emissions from fossil fuel combustion during the Great Recession of 2008–2010, which is consistent with the bottom-up inventory determined by the California Air Resources Board. The isotopic variations and total atmospheric CO₂ from our observations are used to infer seasonality of natural gas and petroleum combustion. For natural gas, inferred emissions are out of phase with the seasonal cycle of total natural gas combustion seasonal patterns in bottom-up inventories but are consistent with the seasonality of natural gas usage by the area's electricity generating power plants. For petroleum, the inferred seasonality of CO₂ emissions from burning petroleum is delayed by several months relative to usage indicated by statewide gasoline taxes. Using the high-resolution Hestia-LA data product to compare emissions from parts of the basin sampled by winds at different times of year, we find that variations in observed fossil fuel CO₂ reflect seasonal variations in wind direction. The seasonality of the local CO₂ excess from fossil fuel combustion along the coast, on Palos Verdes peninsula, is higher in fall and winter than spring and summer, almost completely out of phase with that from Pasadena, also because of the annual variations of winds in the region. Variations in fossil fuel CO₂ signals are consistent with sampling the bottom-up Hestia-LA fossil CO₂ emissions product for sub-city source regions in the LA megacity domain when wind directions are considered.

CO₂ emissions trends in the Los Angeles megacity

S. Newman et al.

Title Page

Abstract

Introduction

Conclusions

References

Tables

Figures



Back

Close

Full Screen / Esc

Printer-friendly Version

Interactive Discussion



1 Introduction

Carbon dioxide is the most important greenhouse gas (GHG) contributing to current global warming, contributing 64 % of the total radiative forcing, according to the IPCC AR5 report (IPCC, 2013) and comprising 82 % of GHG emissions (NRC, 2010). The global average mole fraction of CO₂ has increased approximately 40 % since pre-industrial times due to anthropogenic emissions (IPCC, 2013). Since the proportion of the world's emissions from megacities (urban regions with more than 10 million inhabitants) is out of proportion with their small surface area (EDGAR, 2009; IEA, 2008), quantifying these emissions is essential if we are to work aggressively toward their reduction (Duren and Miller, 2012). As a consequence of global warming mitigation, reducing CO₂ emissions could reduce air pollution mortality, which is correlated with increased CO₂ levels (Jacobson, 2008). Identifying the sources of emissions is a major first step in understanding and mitigating anthropogenic contributions. In cities, these CO₂ sources often dominate over the normally predominant natural source of the biosphere, at least during certain seasons (e.g., Pataki et al., 2003; Widory and Javoy, 2003; Newman et al., 2013, 2008; Lopez et al., 2013; Turnbull et al., 2011, 2015; Vardag et al., 2015). The most common method of inventorying CO₂ emissions from human activities is through bottom-up reporting by governmental agencies, following IPCC methods (IPCC, 2013). This requires self-reporting and may not be reliable in some parts of the world. A more recent, scientifically-based bottom-up approach has been pioneered through the Vulcan and Hestia projects (Gurney et al., 2009, 2012). These efforts combine multiple streams of data such as air pollution reporting, demographics, property tax data, and traffic monitoring, to arrive at what is proving to be a much more accurate and space/time detailed estimate of fossil fuel CO₂ emissions. The Vulcan Project accomplished fossil fuel CO₂ emission estimation for the whole US at spatial scales of 10 km every hour of the year 2002, with updated years expected by the end of 2015. Hestia is specifically focused on the urban domain and has accomplished estimation down to the individual building and street segment scale for four

CO₂ emissions trends in the Los Angeles megacity

S. Newman et al.

Title Page

Abstract

Introduction

Conclusions

References

Tables

Figures



Back

Close

Full Screen / Esc

Printer-friendly Version

Interactive Discussion



CO₂ emissions trends in the Los Angeles megacity

S. Newman et al.

Title Page

Abstract

Introduction

Conclusions

References

Tables

Figures



Back

Close

Full Screen / Esc

Printer-friendly Version

Interactive Discussion



cities (Indianapolis, IN; Salt Lake City, UT; Los Angeles basin, CA; Phoenix, AZ) with work ongoing in Baltimore, MD (Gurney et al., 2012, Patarasuk et al., in prep.; Rao et al., 2015). Both of these detailed data products are available for selected cities in the United States, facilitating top-down emissions quantification through long-term ambient air monitoring (Duren and Miller, 2012; Gurney et al., 2015). Trends in CO₂ emissions must be monitored precisely in order to evaluate progress towards mandated emission reductions. As an example, the California Global Warming Solutions Act of 2006 (Assembly Bill 32) requires reduction of greenhouse gas emissions to 1990 levels by 2020, a reduction of about 15 %. Indeed, now is the time to document the current level of emissions, as governments begin to implement strategies to reduce emissions (e.g., California's Cap-and-Trade Program and Low Carbon Fuel Standards) and want to be able to assess their efficacy.

Within megacities, atmospheric CO₂ concentrations are often highly elevated relative to the regional background due to locally emitted carbon dioxide. This excess can be analyzed for its isotopic composition to help attribute the local emissions to specific processes. Radiocarbon (¹⁴C) analyses give quantitative information as to the proportions of CO₂ resulting from combustion of ancient sources of carbon (fossil fuels) relative to sources incorporating modern carbon, such as the biosphere (e.g., Levin et al., 2003; Levin and Roedenbeck, 2008; Turnbull et al., 2009), because of its short half-life of 5730 years. The stable isotopes of carbon can be used to separate sources with differing values, such as natural gas and petroleum combustion, with the ¹³C/¹²C ratio of natural gas typically being lower than that of petroleum (e.g., Keeling, 1961, 1958; Newman et al., 2008, 2013; Pataki et al., 2003; Widory and Javoy, 2003; Djuricin et al., 2010; Moore and Jacobson, 2015), although there can be overlap between petroleum combustion and biological respiration. Therefore, if we know the biosphere's contribution from the fossil fuel CO₂ contribution derived from Δ¹⁴C and the total CO₂ enhancement over background, we can distinguish all three provided that there are large variations, such as in urban regions.

extraction, manometry, and mass spectrometry. Errors for $\Delta^{14}\text{C}$ average 2‰, based on long-term reproducibility of secondary standards.

2.3 Calculations

A major goal of this study is the attribution of the sources of the CO_2 emissions observed. A schematic figure of the flow of data used to calculate the portion of the total CO_2 that is due to biosphere respiration (bio) and fossil fuel (ff) combustion, including burning of petroleum (pet) and natural gas (ng), is shown in Fig. 2. Mole fractions of CO_2 measured at the two sites and a background site in La Jolla, CA, were used to calculate the CO_2 excess (xs) over background (bg). The contributions of fossil fuel combustion and the biosphere to the excess were determined from radiocarbon measurements, and the fossil fuel component was further broken down into petroleum and natural gas using $\delta^{13}\text{C}$ of the CO_2 . Details are described below.

2.3.1 Total CO_2 emissions and background CO_2 mole fraction

The CO_2 excess caused by local emissions at the two sites was calculated by subtracting an estimate of the background CO_2 mole fraction derived from La Jolla monthly values (Keeling et al., 2005; Figs. 3 and 4). Flask sampling at La Jolla is done so as to minimize the influence of local CO_2 sources by sampling during periods that simultaneously satisfy three criteria: low variability in CO_2 concentration for periods of 3 h or more, wind speed of 2.6 m s^{-1} or more from a narrow southwesterly to westerly sector, and high visibility. That these methods successfully minimize influences of local fossil-fuel emissions is indicated by the consistency of the annual radiocarbon concentrations at La Jolla compared to clean stations both to the north and south in the Northern Hemisphere (Graven, 2012). In this paper, therefore, the La Jolla data presented are screened background data. The La Jolla data were interpolated to determine the appropriate value for the midpoint of the range of collection dates included in each $\Delta^{14}\text{C}$ sample, using the algorithm from Thoning et al. (1989), with two harmonic terms, three

CO_2 emissions trends in the Los Angeles megacity

S. Newman et al.

Title Page

Abstract

Introduction

Conclusions

References

Tables

Figures



Back

Close

Full Screen / Esc

Printer-friendly Version

Interactive Discussion



polynomial terms, and the smoothed residuals of the long term trend (cutoff of 667 days).

2.3.2 CO₂ from fossil fuels, based on Δ¹⁴C

Mass balance calculations were used to calculate the relative contributions of background air, biosphere respiration and photosynthesis, and fossil fuel combustion (including natural gas and oil) to the CO₂ collected at the two sites. The following equations quantitatively separate the background air, biosphere, and fossil fuel combustion contributions to the locally measured atmospheric CO₂ using Δ¹⁴C (e.g., Levin et al., 2003; Miller et al., 2012; Pataki et al., 2003; Turnbull et al., 2006; Fig. 4):

$$C_{\text{obs}} = C_{\text{bg}} + C_{\text{ff}} + C_{\text{r}} + C_{\text{p}} \quad (1)$$

$$\Delta_{\text{obs}} C_{\text{obs}} = \Delta_{\text{bg}} C_{\text{bg}} + \Delta_{\text{ff}} C_{\text{ff}} + \Delta_{\text{r}} C_{\text{r}} + \Delta_{\text{p}} C_{\text{p}} \quad (2)$$

where subscripts obs, bg, ff, r and p indicate observed, background, fossil fuels, respiration, and photosynthesis, respectively, C indicates CO₂ mole fraction in ppm, and Δ indicates Δ¹⁴C in ‰. We assume that Δ_p is equivalent to Δ_{bg} since natural fractionation during uptake is corrected in the Δ¹⁴C measurement and therefore substitute Δ_{bg} for Δ_p in Eq. (2). Then, after solving Eq. (1) for C_{p} and substituting this for C_{p} in Eq. (2), we solve Eq. (2) for C_{ff} , resulting in the following expression for C_{ff} :

$$C_{\text{ff}} = \frac{C_{\text{obs}} (\Delta_{\text{obs}} - \Delta_{\text{bg}})}{\Delta_{\text{ff}} - \Delta_{\text{bg}}} - \frac{C_{\text{r}} (\Delta_{\text{r}} - \Delta_{\text{bg}})}{\Delta_{\text{ff}} - \Delta_{\text{bg}}} \quad (3)$$

The value of Δ_{ff} is −1000 ‰, since fossil fuels contain no ¹⁴C because they have been removed from the source of this short-lived radionuclide for millions of years. We use the record from Pt. Barrow, AK (Xiaomei Xu, unpublished data) for the concurrent background Δ¹⁴C values (Δ_{bg}), because these are the most complete record available for the entire time period of this study. Comparison with the data from La Jolla

**CO₂ emissions
trends in the Los
Angeles megacity**

S. Newman et al.

Title Page

Abstract

Introduction

Conclusions

References

Tables

Figures



Back

Close

Full Screen / Esc

Printer-friendly Version

Interactive Discussion



(Graven et al., 2012; Fig. 5) shows good agreement for 2004–2007, when the two data sets overlap. Comparing the calculated values for C_{ff} from these two backgrounds and propagating through the time series calculations (Sect. 3.4) results in a difference of approximately 1 % of the signal we are measuring. We calculate C_{bio} (the sum of C_r and C_p) from Eq. (1), using the calculated values of C_{ff} and the independent estimates of C_{bg} from the La Jolla data, so that we understand the contribution of the biosphere to total local emissions. The nuclear power plant contribution, the only other source of ^{14}C , is small on the west coast of the US (Graven and Gruber, 2011).

Following Turnbull et al. (2006) and Miller et al. (2012), the respiration terms in the equations above are assumed to reflect contributions due to heterotrophic respiration. Thus, the second term in Eq. (3) is small in magnitude and is due to heterotrophic respiration, through which microbes respire CO_2 that was from carbon previously incorporated through photosynthesis. This term takes into account the isotopic disequilibrium due to the significant time delay between photosynthetic incorporation and respiration, assumed to be 10 years on average (Miller et al., 2012). The magnitude of this correction for our urban Pasadena site is different relative to sites with smaller anthropogenic CO_2 signals, since the CO_2 photosynthesized into the plant a decade ago was not close to the background air composition of that time but was the local, “polluted” air. The Δ_r in Eq. (3) for each sample was calculated by extrapolating the Pasadena trend back 10 years. Because of the mild climate in southern California, we used a constant value of $C_r = 5$ ppm, the same value used for summer by Turnbull et al. (2006). This should be taken as an upper limit for this urban region. The range of the correction for the second term in Eq. (3), including the sign, was -0.06 to -0.11 ppm, generally smaller relative to regions where the biosphere contribution C_r is large (Miller et al., 2012; Turnbull et al., 2006). For the data from the Palos Verdes site, we calculated the heterotrophic correction term using values of Δ_r calculated by extrapolating the Pt. Barrow background trend back 10 years and used a constant value of $C_r = 5$ ppm, because of the mild climate. The correction term for the Palos Verdes data ranged from

0.20–0.24 ppm. The small correction for heterotrophic respiration does not affect any of our conclusions.

In California, there is an added complication when attributing CO₂ emissions to fossil fuels using Δ¹⁴C. Since 2004, 10 % ethanol has been added to gasoline. The ethanol contains modern, not fossil, carbon. For gasoline with 10 % ethanol, 6.7 % of the CO₂ emitted during combustion is from the modern ethanol (EIA, 2015). A correction for this is made, as discussed in Sect. 2.3.3 below.

2.3.3 δ¹³C of CO₂

Plots involving the mole fractions and δ¹³C can be used to determine δ¹³C of the local contribution to the observed CO₂ (Fig. 3). Here we use the Miller–Tans approach (Miller–Tans approach; MT; Miller and Tans, 2003) for this purpose, since it allows for variations in background composition and we observe a widening difference between the data for δ¹³C in Pasadena and the La Jolla background record in recent years (Fig. 3e). The following mass balance equations are used in this analysis:

$$C_{\text{obs}} = C_{\text{bg}} + C_{\text{src}} \quad (4)$$

$$\delta_{\text{obs}} \times C_{\text{obs}} = \delta_{\text{bg}} \times C_{\text{bg}} + \delta_{\text{src}} \times C_{\text{src}} \quad (5)$$

to give

$$\delta_{\text{obs}} \times C_{\text{obs}} - \delta_{\text{bg}} \times C_{\text{bg}} = \delta_{\text{src}}(C_{\text{obs}} - C_{\text{bg}}) \quad (6)$$

(Miller and Tans, 2003), where the subscript src represents the local source of CO₂ emissions, δ represents δ¹³C, and the appropriate background values are included for each sample. Using this formulation (Eq. 6), the slope of the correlation (MT slope) gives the δ¹³C of this local source. For this analysis, we calculated the MT slopes for each month and then determined the seasonal averages, averaging December–January–February as winter, March–April–May as spring, June–July–August as summer, and September–October–November as autumn. Seven individual samples, over

CO₂ emissions trends in the Los Angeles megacity

S. Newman et al.

Title Page

Abstract

Introduction

Conclusions

References

Tables

Figures



Back

Close

Full Screen / Esc

Printer-friendly Version

Interactive Discussion



the eight-year sampling period in Pasadena, were excluded since they fell more than three times the standard error from their linear regression best-fit lines. The monthly MT plots for 2011 are shown in Fig. A1, as examples.

We use the results from the $^{14}\text{CO}_2$ calculations for the fraction of C_{xs} from the biosphere ($F_{\text{bio}} = 1 - F_{\text{ff}}$) together with the MT slopes to attribute the CO_2 derived from petroleum and natural gas combustion (C_{pet} and C_{ng}) by mass balance, first by calculating the $\delta^{13}\text{C}$ of the fossil fuel component, using:

$$\delta_{\text{ff}} = \frac{\delta_{\text{xs}} - \delta_{\text{bio}} \times (1 - F_{\text{ff}})}{F_{\text{ff}}} \quad (7)$$

where F_{ff} is the fraction of C_{xs} due to emissions from fossil fuel combustion, as calculated from the $^{14}\text{CO}_2$ data. The values for δ_{xs} are the seasonal $\delta^{13}\text{C}$ values from the MT analyses and δ_{bio} is taken to be -26.6‰ , the average $\delta^{13}\text{C}$ of the ambient air plus the discrimination of -16.8‰ for the biosphere (Bakwin et al., 1998). Then the proportions of CO_2 emitted by petroleum and natural gas combustion are calculated using the $\delta^{13}\text{C}$ values:

$$\delta_{\text{ff}} = F_{\text{petff}} \times \delta_{\text{pet}} + (1 - F_{\text{petff}}) \times \delta_{\text{ng}} \quad (8)$$

$$F_{\text{petff}} = \frac{\delta_{\text{ff}} - \delta_{\text{ng}}}{\delta_{\text{pet}} - \delta_{\text{ng}}} \quad (9)$$

with an analogous equation for F_{ngff} where F_{petff} and F_{ngff} are the fractions of petroleum and natural gas combustion contributions in C_{ff} , respectively. The values of δ_{ng} and δ_{pet} used were -40.2‰ for natural gas (Newman et al., 2008) and -25.5‰ for petroleum combustion (average of measurements in Newman et al., 2008, and -25.1‰ measured in 2012). The C_{ff} , C_{pet} , and C_{bio} components were corrected for the presence of 10% ethanol in California gasoline by multiplying C_{pet} by 0.067 (the fraction of CO_2 emitted by burning the ethanol portion of the ethanol-gasoline mixture; EIA, 2015) to

CO₂ emissions trends in the Los Angeles megacity

S. Newman et al.

Title Page

Abstract

Introduction

Conclusions

References

Tables

Figures



Back

Close

Full Screen / Esc

Printer-friendly Version

Interactive Discussion



give the amount, in ppm, of CO₂ that was included in C_{bio} but should have been attributed to C_{pet} . The same amount was deducted from C_{bio} . The magnitude of this correction is 0.5–1.2 ppm.

2.3.4 Time series analysis

We used the algorithm of Jiang et al. (2008) to study details of the average annual patterns of the total CO₂ and C_{ff} in Pasadena, in order to compare with patterns at sites with less contribution from regional fossil fuel combustion, such as Palos Verdes and La Jolla background. This method uses the first three Legendre polynomials and harmonic terms to decompose the signal (Prinn et al., 2000). The harmonic terms define the seasonal and semi-annual cycles, which we compared to results of the same analysis for flask data from La Jolla, CA (Keeling et al., 2005).

To determine trends in the C_{ff} time series, derived from the radiocarbon data, we used the empirical mode decomposition (EMD) method (Huang et al., 1998; Kobayashi-Kirschvink et al., 2012). Using this method, nonlinear and nonstationary time series can be broken down into intrinsic mode functions (IMFs) with increasing period lengths and, finally, to a long-term trend with at most only one minimum or maximum with slope of zero. Following Wu and Huang (2009), we added random noise equivalent to the error in the measurements to create 300 time series, for which the ensemble EMD (EEMD) analyses were averaged. The EEMD technique is data adaptive, not assuming any shape for the IMFs.

3 Results and discussion

The purpose of this project was to determine the sources of CO₂ emissions in the Los Angeles basin and compare them with bottom-up inventories from government agencies and the scientific community. Below, we compare results of source allocation from the two sites and then examine the temporal variability at the Pasadena site, with

CO₂ emissions trends in the Los Angeles megacity

S. Newman et al.

Title Page

Abstract

Introduction

Conclusions

References

Tables

Figures



Back

Close

Full Screen / Esc

Printer-friendly Version

Interactive Discussion



its 8 year record. Then we compare the results with government inventories and with the high-resolution Hestia-LA emissions product.

3.1 Spatial variations – comparison of source attribution at the Pasadena and Palos Verdes sites

5 The $\Delta^{14}\text{C}$ time series for the two sites are shown in Fig. 3c and d, 8 years for Pasadena and 4 years for Palos Verdes. The two data sets are very different, with Palos Verdes radiocarbon results being significantly higher than those in Pasadena except during the winter. The summer months in Pasadena are characterized by $\Delta^{14}\text{C}$ values far from background, i.e., depleted in ^{14}C due to dilution by CO_2 produced by burning of
10 fossil fuels containing none of the radioactive isotope. There are occasional negative spikes in $\Delta^{14}\text{C}$ during the winter. Total CO_2 excess (C_{xs} ; Fig. 4), determined as CO_2 concentration minus background, is similarly disparate with respect to timing. The total enhancement at both Pasadena and Palos Verdes, C_{xs} , spikes during winter (up to 65 and 34 ppm, respectively), but the Pasadena excess also peaks during the summer (up to 43 ppm), whereas Palos Verdes values for C_{xs} are at a minimum during the warm
15 months (3–20 ppm). When the ^{14}C and C_{xs} information are combined to calculate CO_2 emissions due to fossil fuels (C_{ff} ; Eq. 3; Fig. 4), we see summer maxima for C_{ff} in Pasadena, but not in Palos Verdes. The spikes in C_{xs} and C_{ff} during fall and winter seasons are not the general trend in Pasadena, as evidenced by the quarterly averages (Fig. 6b). The amount of C_{ff} in the Pasadena seasonal averages (Figs. 4a and 6b) ranges from (18.9 ± 1.2) ppm (winter) to (26.8 ± 0.4) ppm (summer). In Palos Verdes, C_{ff} averages (5 ± 3) ppm during the warmer months and (12 ± 5) ppm during the winter months (Fig. 4b). However, CO_2 emissions from the biosphere (C_{bio}) tend to be higher during the cooler months at both sites (Fig. 4).

25 The explanation for the differences in the seasonal cycles of C_{xs} and C_{ff} at the two sites is probably the different wind patterns for the different times of year. Figure 7 shows back trajectories ending at 14:00 PST in Pasadena (Fig. A2 for both sites), calculated using NOAA's HYSPLIT model (Draxler and Rolph, 2014.), for January and

CO₂ emissions trends in the Los Angeles megacity

S. Newman et al.

[Title Page](#)[Abstract](#)[Introduction](#)[Conclusions](#)[References](#)[Tables](#)[Figures](#)[Back](#)[Close](#)[Full Screen / Esc](#)[Printer-friendly Version](#)[Interactive Discussion](#)

July 2011. These are representative of these months in all years of this study. Wind directions during July are from the west-southwest, whereas they are mostly from the northeast but much more varied during the winter. Thus, in Pasadena, elevated C_{xs} and C_{ff} values during the summer result from air masses traveling across the Los Angeles basin, picking up emissions and transporting them inland. During the winter, the airflow is more mixed, resulting in lower average C_{ff} signals in Pasadena, since a significant proportion of the winds bring less polluted air from the much less populated mountains and deserts located to the north (Santa Ana winds) (Fig. 7). The summer westerly winds bring ocean air to the Palos Verdes site, characterized by CO₂ mole fractions and $\Delta^{14}\text{C}$ very similar to background marine air. During the cooler months, the Santa Ana winds from the northeast occasionally blow over the LA basin, bringing its emissions to the coastal site (Fig. 7). This pattern results in more scatter in the magnitude of CO₂ excess observed during the winter at the Palos Verdes site, than during the summer. Figure 8 shows the average annual patterns for C_{ff} at the two sites, demonstrating the effect of the varying wind direction patterns.

3.2 Attribution of CO₂ excess from different anthropogenic sources for Pasadena

Since we have information regarding the relative contributions of fossil fuel combustion and biosphere respiration from the radiocarbon data, we can use the differences in the $\delta^{13}\text{C}$ of the CO₂ to look at the contributions of petroleum/gasoline vs. natural gas combustion. We use the MT approach to distinguish between different fossil fuel sources of CO₂ (Miller and Tans, 2003). As described in Sect. 2.3.3, the MT slope of the correlation gives the $\delta^{13}\text{C}$ of the local source of CO₂ emissions. In many cases it is difficult to distinguish the anthropogenic sources because the biosphere's signal can overlap that of petroleum. However, in a megacity such as the Los Angeles basin, the contribution of the biosphere to the total CO₂ enhancement can be minimal ($\leq 20\%$ in Pasadena; Newman et al., 2008, 2013) during the afternoon, when the boundary

layer is deepest and most thoroughly mixed. In this study, we use the information from $\Delta^{14}\text{C}$ presented above to further constrain the biosphere's input. Since the other major anthropogenic sources (cement production and combustion of coal) are not present in the Los Angeles basin, $\delta^{13}\text{C}$ from MT plots can be used to differentiate the proportions of natural gas and oil burned in the region, as discussed below.

Seasonal MT slopes for the mid-afternoon Pasadena samples from 2006 through 2013 are shown in Fig. 6a. We do not present similar analysis for the Palos Verdes data because it is a shorter data set, with only 3–5 measurements per month (12 per season), and the range in CO_2 mole fractions during the warmer months is less than 20 ppm for all spring and summer seasons. Thus there are insufficient meaningful data to produce a significant trend. Vardag et al. (2015) came to this same conclusion for a rural site in Germany, based on a modeling study.

The $\delta^{13}\text{C}$ values from MT regressions for the cooler portions of the year in Pasadena are almost always higher than those for the warmer portions. The values for the cooler seasons average $(-30.6 \pm 0.5)\text{‰}$, 1.8‰ higher than the average for the warmer months, $(-32.4 \pm 0.6)\text{‰}$. Newman et al. (2008) showed that no biospheric input was required to explain the $\delta^{13}\text{C}$ of mid-afternoon CO_2 during 1972–1973 and 2002–2003, although up to 20% was allowed by the uncertainties. Assuming that there is no contribution from respiration and that the $\delta^{13}\text{C}$ of the high- CO_2 end members are -40.2‰ for natural gas and -25.5‰ for petroleum combustion, as discussed above, then the proportion of natural gas burned in C_{XS} is 32% during the cooler months and 45% during the warmer months. The larger fraction of natural gas burned during the warm part of the year is consistent with the observed burning of more natural gas for electricity generation during summer months, as would be required to power air conditioning needs. Mild winters in this climate require less natural gas combustion for heating buildings, thus minimizing a large winter peak frequently seen in colder regions, such as Salt Lake City, UT (Pataki et al., 2003; Bush et al., 2007) and Chicago, IL (Moore and Jacobson, 2015).

CO₂ emissions trends in the Los Angeles megacity

S. Newman et al.

Title Page

Abstract

Introduction

Conclusions

References

Tables

Figures



Back

Close

Full Screen / Esc

Printer-friendly Version

Interactive Discussion



**CO₂ emissions
trends in the Los
Angeles megacity**

S. Newman et al.

Title Page

Abstract

Introduction

Conclusions

References

Tables

Figures



Back

Close

Full Screen / Esc

Printer-friendly Version

Interactive Discussion



analysis of Jiang et al. (2008; Fig. 9b and h). The sum of the seasonal and semi-annual harmonic terms reproduces the data very well, with R^2 values of 0.70 and 0.91 for Pasadena and background, respectively. The average annual cycles are 6 months out of phase, whereas the semi-annual oscillation cycles look very similar at the two sites.

The seasonal cycle in Pasadena is consistent with influx of combustion CO₂ during the hot summer months due to increased burning of natural gas at power plants located dominantly in the southwestern portion of the LA basin (CEC, 2015). In contrast, the background data reflect global patterns with a drawdown in CO₂ during the summer growing season in the Northern Hemisphere. Jiang et al. (2012) concluded that the semi-annual oscillation at NOAA's GLOBAL-VIEW sites is due to the combination of net primary production and respiration of the biosphere. The semi-annual oscillation in the background signal is consistent with this interpretation. We see virtually the same pattern in Pasadena, although the amplitude is smaller, consistent with the small biospheric contribution indicated by the $\Delta^{14}\text{C}$ results.

Based on the work of Jiang et al. (2012) we expect the annual cycle in Pasadena to be larger in amplitude than in La Jolla since it is further north, but the amplitude is actually much smaller. If the regional emissions of CO₂ in Pasadena are relative to a La Jolla background, then there is a huge enhancement during the summer! Indeed, the seasonal cycle for C_{ff} (Fig. 8) is 11 ppm, with the peak in August–September, and there is very little semi-annual oscillation.

The annual pattern for CO₂ in Palos Verdes is also heavily influenced by the transport of combustion emissions from the Los Angeles basin (Figs. 7, 8, 9c and d). The average monthly pattern is more similar to the background's (Fig. 9g and h) than to Pasadena's (Fig. 9a and b). However, there is a strong peak in the winter that is consistent with the increased number of days during this time of year with winds from the north to east, travelling over the basin. Doing the same analysis for the monthly minimum values (Fig. 9e and f) gives a pattern that is much more similar to the background's, confirmed by the comparison of the raw data with the background smoothed time series in Fig. 3. This supports use of minimum values from Palos Verdes as reasonable background

for the Los Angeles basin. The C_{ff} annual pattern is inverse to that in Pasadena, as expected by the seasonal wind patterns (Figs. 7 and 8).

The conclusion of this analysis of the annual cycles is that the Pasadena CO_2 pattern is significantly different from the natural cycles observed in La Jolla background and show very little seasonal variation compared with this background. The semi-annual pattern, although smaller in amplitude than expected, is in phase with that observed in the background, probably reflecting a reduced biosphere signature in Pasadena due to artificial irrigation. Both the Pasadena and Palos Verdes average CO_2 patterns reflect the seasonal changes in wind patterns, whereas the monthly minimum Palos Verdes pattern is that expected for the background air entering the LA basin. It will be interesting to see whether water restrictions put into effect during summer of 2015 because of an on-going, severe drought (ca.gov/drought, 2015), affect the patterns observed in the future.

3.4 Temporal trends in CO_2 excess observed in Pasadena

3.4.1 Long-term time series analysis

In order to discern the long-term trends in fossil-fuel CO_2 excess, we must first remove noise and the periodic signals discussed above from the record. We used empirical mode decomposition (EEMD; Huang et al., 1998; Kobayashi-Kirschvink et al., 2012), as described in the calculation section above, on the 8 year time series of C_{ff} (Fig. 4a) to identify intrinsic mode functions (IMFs; summary in Fig. 10a–d; full results in Fig. A3). The noise is represented by the first and second modes (IMF 1 and IMF 2). Combination of the third and fourth modes of the C_{ff} time series (IMF 3 and IMF 4) correlates significantly with the 30 day average record for temperature measured at the top of the 9-story library next to the sampling site ($R^2 = 0.6$). Because the time series is so clearly dominated by the annual cycle, we then subtracted the average annual cycle, averaged by month over the entire time period (2006–2013) (resulting time series shown in Fig. 10e). The EEMD was calculated again in order to determine the inter-annual trend

CO_2 emissions trends in the Los Angeles megacity

S. Newman et al.

Title Page

Abstract

Introduction

Conclusions

References

Tables

Figures



Back

Close

Full Screen / Esc

Printer-friendly Version

Interactive Discussion



CO₂ emissions trends in the Los Angeles megacity

S. Newman et al.

Title Page

Abstract

Introduction

Conclusions

References

Tables

Figures



Back

Close

Full Screen / Esc

Printer-friendly Version

Interactive Discussion



(Fig. 10f). The sum of the trend + IMF 6 is a curve with increasing C_{ff} values leading up to mid-2007, when they began to fall, until leveling off in 2010 and perhaps starting to rise towards the end of the time series. There are end effects in this method, such that we do not have confidence in the first and last years of the analysis. The uncertainties in this calculation are shown by the shaded regions in Fig. 10f. These were determined as the 1σ standard deviations of adding random noise equivalent to 13.7 % to the data 300 times and then running the EMD analysis. The 13.7 % noise added is the uncertainty of the C_{ff} values calculated from $\Delta^{14}C$, ± 1 ppm, relative to the standard deviation of the data, 7.3 ppm. The maximum and minimum values are distinct at approximately the 2σ standard deviation level, as shown in Fig. 10f and indicate a significant decrease of 9.5 % between the maximum in May 2007 (average from Fig. 10a plus the maximum in Fig. 10f: 23.7 ppm) and the average for January–June 2010 (average from Fig. 10a plus the average of minimum six-month period from Fig. 10f: 21.4 ppm). Using different backgrounds for $\Delta^{14}C$, such as extrapolating the data from La Jolla (Fig. 5) does not significantly affect this analysis, resulting in differences of (0.01 ± 0.09) ppm C_{ff} out of a range on the order of 2 ppm. And our result showing that there are different values of $\Delta^{14}C$ for bulk fuel for autumn–winter than for spring–summer also does not change these conclusions, since the RMSE of the IMF6+ trend (Fig. 10f) using different $\Delta^{14}C$ for cool vs. summer months relative to the constant average value is 0.1 ppm C_{ff} .

The timing of the drop in the fossil-fuel CO₂ excess around 2008 is consistent with the economic recession in late 2007–2009 (NBER, 2010) with slow recovery beginning in 2010. Similar results for global CO₂ emissions due to fossil fuel combustion have been documented by Peters et al. (2012) and Asefi-Najafabady et al. (2014). The fraction of decrease in C_{ff} (9.5 %) is similar to, although less than, the decrease in global GDP during this time (global GDP decreased by 13 %; World Bank, 2015). The observation that C_{ff} does not decrease by as large a percentage as the economy is consistent with the analysis of York (2012) that anthropogenic emissions are asymmetric with respect to economic growth and decline. Increases in emissions that come during growth periods are not matched by declines of the same magnitude during economic downturns, be-

tion data, based on deliveries (EIA), and gasoline taxes collected (CBE, 2014) with C_{pet} indicates similar decreases of 10–20 %, but with a lag of a few months (Fig. 12). The EIA and State of California data reflect the entire state domain while the Hestia emissions data product reflects the LA Basin specifically. Furthermore, the EIA data and the gasoline tax-based data will likely be displaced in space and time from the point of combustion, which is dominated by on-road vehicles. The Hestia data, by contrast, is a fossil fuel CO_2 emissions data product specific in space and time to the individual building and road segments (Gurney et al., 2012).

To truly understand the observations in Pasadena, we must combine information from spatial and temporal meteorological and emissions databases, such as obtained using a model like the Weather Research and Forecasting (WRF) model. Since this is beyond the scope of this work, we have used the information from HYSPLIT back trajectories (Fig. 7; January and July) to provide rough limits for winds arriving in Pasadena at our sampling time of 14:00 PST. These back trajectories suggest that prevailing winds during the summer come from the southwest, across the basin, and winds during the winter come from the northeast, across the mountains from the desert. We have looked at $1.3\text{ km} \times 1.3\text{ km}$ gridded emissions from the Hestia-LA data product to qualitatively determine what relative emissions from petroleum combustion are expected during January and July for the two years of the Hestia data (2011 and 2012). These are plotted in Fig. 12 and agree with the observations presented here, that more C_{pet} is observed during the summer than during the winter. A map of the regions selected for January (NE) and July (SW) is presented in Fig. 13a, along with the HYSPLIT back trajectories for January and July 2011, and the monthly average CO_2 emissions due to total petroleum combustion (the Hestia-LA product) from the two integrated areas based on the wind directions are shown in Fig. 13b for years 2011 and 2012.

We show comparison of the C_{ng} results from Pasadena with area-integrated bottom-up inventories and the Hestia-LA data product in Fig. 14. The California Energy Commission (CEC, 2015) compiles data for natural gas consumed by power plants throughout the state, including Los Angeles and Orange counties. These seasonal data are

CO₂ emissions trends in the Los Angeles megacity

S. Newman et al.

Title Page

Abstract

Introduction

Conclusions

References

Tables

Figures



Back

Close

Full Screen / Esc

Printer-friendly Version

Interactive Discussion



concentrate on the longer-term signals, which show reasonable agreement with the longer-term trends in the statewide inventory.

4 Conclusion

Detection of anthropogenic excess of CO₂ at two sites in the Los Angeles basin, one on the coast and one inland against a barrier mountain range, reveals significant spatial and seasonal variability due to the biosphere, natural gas combustion, and petroleum combustion. Seasonal patterns in wind direction determine the source region of the excess detected at the two sites. Winds from the west to southwest during the warmer months bring marine air with little excess to Palos Verdes, and these same winds continue across the LA basin picking up emissions from fossil fuel combustion to be observed in Pasadena. During the cooler months, wind directions are more varied and include periods when air with low emissions comes to Pasadena from the northeast to northwest and then travels across the basin to Palos Verdes, incorporating anthropogenic emissions along the way.

The nature of the excess changes with season, as reflected by the $\delta^{13}\text{C}$ values of CO₂ observed in Pasadena. During warmer months, lower values for $\delta^{13}\text{C}$ of the local excess indicate a higher proportion of natural gas burned, consistent with government inventories that indicate more natural gas burned during summer to produce electricity to power air conditioning. Even more importantly, however, the seasonal trends in the fossil fuel combustion observed in Pasadena are consistent with the shift from south-westerly winds during warmer months to northeasterly winds during cooler months. Therefore the source region of emissions changes from the Los Angeles basin during summer to the mountains and desert during winter, for our Pasadena sampling site. Trend analysis by ensemble empirical mode decomposition supports the relationship between emissions and temperature.

The long-term trend in CO₂ excess from fossil fuel combustion is consistent with emissions changes associated with the economic recession and slow recovery of 2008

CO₂ emissions trends in the Los Angeles megacity

S. Newman et al.

Title Page

Abstract

Introduction

Conclusions

References

Tables

Figures



Back

Close

Full Screen / Esc

Printer-friendly Version

Interactive Discussion



CO₂ emissions trends in the Los Angeles megacity

S. Newman et al.

Title Page

Abstract

Introduction

Conclusions

References

Tables

Figures



Back

Close

Full Screen / Esc

Printer-friendly Version

Interactive Discussion



through the present, and indicates a significant decrease of 9.5 % since the maximum in late 2007, consistent with the bottom-up inventory of the California Air Resources Board. Indeed, top-down and bottom-up methods of determining the anthropogenic sources of CO₂ emissions must be compared to each other to better understand inconsistencies, potential biases, and uncertainty. Previously, however, comparisons have been limited by the scope of emissions, large and overlapping uncertainty, and differences in the target domain. Here we have shown that combining data from radiocarbon and $\delta^{13}\text{C}$ values moves us towards a direct comparison in a megacity with very large emissions. Measurement trends at a receptor site are consistent with annual variations in California statewide bottom-up inventories for CO₂ emissions attributed to petroleum and natural combustion, individually as well as for total CO₂ emissions. Even greater consistency between top-down measurements and granular emission estimates specific for the LA megacity domain are achieved when considering wind direction and sub-city source regions. This strengthens the need to have measurement, modeling, and inventories that are specifically aimed at the same domain with fine space/time resolution.

The next steps are to include modeling with inversion of the measurements to understand the combination of atmospheric transport and emissions and to extend the analysis to a denser network of surface monitoring stations such as the Los Angeles Megacities Carbon Monitoring Project (Kort et al., 2013) and the California Laboratory for Atmospheric Remote Sensing (CLARS) observations from Mount Wilson (Wong et al., 2015). Although the uncertainties are large enough that the method described here will not be usable in non-urban regions, similar to the conclusion of the modeling study by Vardag et al. (2015), anthropogenic emissions dominate significantly over natural processes in megacities. Therefore, this kind of monitoring in megacities will allow society to understand and monitor the sources of the CO₂ that are the major contributors to global warming.

Acknowledgements. This work would not have been possible without support from the W.M. Keck Carbon Cycle Facility at UCI. We specifically thank J. Southon for his help with sample analysis. We acknowledge funding from the Keck Institute for Space Studies, NASA Grant NNX13AC04G, and NASA Grant NNX13AK34G. We also acknowledge funding from the California Air Resources Board Contract #13-329. The statements and conclusions in this report are those of the Contract and not necessarily those of the California Air Resources Board. The mention of commercial products, their source, or their use in connection with materials reported herein is not to be construed as actual or implied endorsement of such products. The authors gratefully acknowledge the NOAA Air Resources Laboratory (ARL) for providing the HYSPLIT transport and dispersion model used in this publication. We thank N. C. Shu for hosting the site on the Palos Verdes peninsula.

References

- Affek, H. and Eiler, J.: Abundance of mass 47 CO₂ in urban air, car exhaust, and human breath, *Geochim. Cosmochim. Ac.*, 70, 1–12, 2006.
- Asefi-Najafabady, S., P. J. Rayner, K. R. Gurney, A. McRobert, Y. Song, K. Coltin, J. Huang, C. Elvidge, and K. Baugh: A multiyear, global gridded fossil fuel CO₂ emission data product: evaluation and analysis of results, *J. Geophys. Res.-Atmos.*, 119, 213–10, doi:10.1002/2013JD021296, 2014.
- Bakwin, P., Tans, P., White, J., and Andres, R.: Determination of the isotopic (¹³C/¹²C) discrimination by terrestrial biology from a global network of observations, *Global Biogeochem. Cy.*, 12, 555–562, 1998.
- Bush, S., Pataki, D., and Ehleringer, J.: Sources of variation in δ¹³C of fossil fuel emissions in Salt Lake City, USA, *Appl. Geochem.*, 2, 715–723, doi:10.1016/j.apgeochem.2006.11.001, 2007.
- CARB: California Air Resources Board: available at: <http://www.arb.ca.gov/cc/inventory/data/data.htm> (last access: July 2015), 2015.

CO₂ emissions trends in the Los Angeles megacity

S. Newman et al.

Title Page

Abstract

Introduction

Conclusions

References

Tables

Figures



Back

Close

Full Screen / Esc

Printer-friendly Version

Interactive Discussion



CO₂ emissions trends in the Los Angeles megacity

S. Newman et al.

Title Page

Abstract

Introduction

Conclusions

References

Tables

Figures



Back

Close

Full Screen / Esc

Printer-friendly Version

Interactive Discussion



- CBE: California Board of Equalization: available at: http://www.boe.ca.gov/sptaxprog/reports/MVF_10_Year_Report.pdf (last access: November 2014), 2014.
- CEC: California Energy Commission: available at: http://energyalmanac.ca.gov/electricity/web_qfer/Power_Plant_Statistical_Information.php (last access: January 2015), 2015.
- 5 Clark-Thorne, S. and Yapp, C.: Stable carbon isotope constraints on mixing and mass balance of CO₂ in an urban atmosphere: Dallas metropolitan area, Texas, USA, *Appl. Geochem.*, 18, 75–95, 2003.
- Djuricin, S., Pataki, D. E., and Xu, X.: A comparison of tracer methods for quantifying CO₂ sources in an urban region, *J. Geophys. Res.-Atmos.*, 115, D11303, doi:10.1029/2009JD012236, 2010.
- 10 Draxler, R. R. and Rolph, G. D.: HYSPLIT (HYbrid Single-Particle Lagrangian Integrated Trajectory) Model access via NOAA ARL READY Website (<http://www.arl.noaa.gov/HYSPLIT~T.php>), NOAA Air Resources Laboratory, College Park, MD, 2014.
- Duren, R. M. and Miller, C. E.: Measuring the carbon emissions of megacities, *Nature Climate Change*, 2, 560–562, 2012.
- 15 EDGAR: European Commission, Joint Research Centre (JRC)/Netherlands Environmental Assessment Agency (PBL), Emission Database for Global Atmospheric Research (EDGAR), release version 4.0. available at: <http://edgar.jrc.ec.europa.eu> (last access: September 2015), 2009.
- 20 EIA (US Energy Information Agency): Frequently asked questions: available at: <http://www.eia.gov/tools/faqs/faq.cfm?id=307&t=11>, last access: 4 September 2015.
- Gonfiantini, R.: Standards for stable isotope measurements in natural compounds, *Nature*, 271, 534–536, 1978.
- Graven, H. D. and Gruber, N.: Continental-scale enrichment of atmospheric ¹⁴CO₂ from the nuclear power industry: potential impact on the estimation of fossil fuel-derived CO₂, *Atmos. Chem. Phys.*, 11, 12339–12349, doi:10.5194/acp-11-12339-2011, 2011.
- 25 Graven, H. D., Guilderson, T. P., and Keeling, R. F.: Observations of radiocarbon in CO₂ at La Jolla, California, USA 1992–2007: analysis of the long-term trend, *J. Geophys. Res.*, 117, D02302, doi:10.1029/2011JD016533, 2012.
- 30 Gurney, K. R., Razlivanov, I., Song, Y., Zhou, Y., Benes, B., and Abdul-Massin, M.: Quantification of fossil fuel CO₂ emissions on the building/street scale for a large US city, *Environ. Sci. Technol.*, 46, 12194–12202, doi:10.1021/es3011282, 2012.

CO₂ emissions trends in the Los Angeles megacity

S. Newman et al.

Title Page

Abstract

Introduction

Conclusions

References

Tables

Figures



Back

Close

Full Screen / Esc

Printer-friendly Version

Interactive Discussion



Gurney, K. R., Romero-Lankao, P., Seto, K. C., Hutyra, L. R., Duren, R., Kennedy, C., Grimm, N. B., Ehleringer, J. R., Marcutuillio, P., Hughes, S., Pincetl, S., Chester, M. V., Runfola, D. M., Feddema, J. J., and Sperling, J.: Climate change: track urban emissions on a human scale, *Nature*, 525, 179–181, doi:10.1038/525179a, 2015.

Huang, N., Shen, Z., and Long, S.: The empirical mode decomposition and the Hilbert spectrum for nonlinear and non-stationary time series analysis, *P. Roy. Soc. Lond. A*, 454, 903–995, 1998.

IEA: World Energy Outlook 2008, edited by: F. Birol, International Energy Agency, 2008.

IPCC: Climate Change 2013: The Physical Science Basis. Contribution of Working Group I to the Fifth Assessment Report of the Intergovernmental Panel on Climate Change, edited by: Stocker, T. F., Qin, D., Plattner, G.-K., Tignor, M., Allen, S. K., Boschung, J., Nauels, A., Xia, Y., Bex, V., and Midgley, P. M., Cambridge University Press, Cambridge, UK and New York, NY, USA, 1535 pp., 2013.

Jacobson, M. Z.: On the causal link between carbon dioxide and air pollution mortality, *Geophys. Res. Lett.*, 35, L03809, doi:10.1029/2007GL031101, 2008.

Jiang, X., Li, Q., Liang, M.-C., Shia, R.-L., Chahine, M. T., Olsen, E. T., Chen, L. L., and Yung, Y. L.: Simulation of upper tropospheric CO₂ from chemistry and transport models, *Global Biogeochem. Cy.*, 22, GB4025, doi:10.1029/2007GB003049, 2008.

Jiang, X., Chahine, M. T., Li, Q., Liang, M., Olsen, E. T., Chen, L. L., Wang, J., and Yung, Y. L.: CO₂ semiannual oscillation in the middle troposphere and at the surface, *Global Biogeochem. Cy.*, 26, GB3006, doi:10.1029/2011GB004118, 2012.

Keeling, C.: The concentration and isotopic abundances of carbon dioxide in rural and marine air, *Geochim. Cosmochim. Ac.*, 24, 277–298, 1961.

Keeling, C. D.: The concentration and isotopic abundances of atmospheric carbon dioxide in rural areas, *Geochim. Cosmochim. Ac.*, 13, 322–334, doi:10.1016/0016-7037(58)90033-4, 1958.

Kobayashi-Kirschvink, K. J., Li, K.-F., Shia, R.-L., and Yung, Y. L.: Fundamental modes of atmospheric CFC-11 from empirical mode decomposition, *Adv. Adapt. Data. Anal.*, 04, 1250024, doi:10.1142/S1793536912500240, 2012.

Kort, E. A., Angevine, W., Duren, R., and Miller, C. E.: Surface observations for monitoring urban fossil fuel CO₂ emissions: minimum site location requirements for the Los Angeles megacity, *J. Geophys. Res.*, 118, 1–8, doi:10.1002/jgrd.50135, 2013.

CO₂ emissions trends in the Los Angeles megacity

S. Newman et al.

Title Page

Abstract

Introduction

Conclusions

References

Tables

Figures



Back

Close

Full Screen / Esc

Printer-friendly Version

Interactive Discussion



- Levin, I. and Roedenbeck, C.: Can the envisaged reductions of fossil fuel CO₂ emissions be detected by atmospheric observations?, *Naturwissenschaften*, 95, 203–208, doi:10.1007/s00114-007-0313-4, 2008.
- Levin, I., Kromer, B., Schmidt, M., and Sartorius, H.: A novel approach for independent budgeting of fossil fuel CO₂ over Europe by ¹⁴CO₂ observations, *Geophys. Res. Lett.*, 30, 2194, doi:10.1029/2003GL018477, 2003.
- Lopez, M., Schmidt, M., Delmotte, M., Colomb, A., Gros, V., Janssen, C., Lehman, S. J., Mondelain, D., Perrussel, O., Ramonet, M., Xueref-Remy, I., and Bousquet, P.: CO, NO_x and ¹³CO₂ as tracers for fossil fuel CO₂: results from a pilot study in Paris during winter 2010, *Atmos. Chem. Phys.*, 13, 7343–7358, doi:10.5194/acp-13-7343-2013, 2013.
- Lu, R. and Turco, R.: Air pollutant transport in a coastal environment. Part I: Two-dimensional simulations of sea-breeze and mountain effects, *J. Atmos. Sci.*, 51, 2285–2308, 1994.
- Lu, R. and Turco, R.: Air pollutant transport in a coastal environment – I. I. Three-dimensional simulations over Los Angeles basin, *Atmos. Environ.*, 29, 1499–1518, 1995.
- Miller, J. and Tans, P.: Calculating isotopic fractionation from atmospheric measurements at various scales, *Tellus B*, 55, 207–214, 2003.
- Miller, J. B., Lehman, S. J., Montzka, S. A., Sweeney, C., Miller, B. R., Karion, A., Wolak, C., Dlugokencky, E. J., Southon, J., Turnbull, J. C., and Tans, P. P.: Linking emissions of fossil fuel CO₂ and other anthropogenic trace gases using atmospheric ¹⁴CO₂, *J. Geophys. Res.*, 117, D08302, doi:10.1029/2011JD017048, 2012.
- Moore, J. and Jacobson, A. D.: Seasonally varying contributions to urban CO₂ in the Chicago, Illinois, USA region: insights from a high-resolution CO₂ concentration and δ¹³C record, *Elem. Sci. Anth.*, 3, 000052, doi:10.12952/journal.elementa.000052.s004, 2015.
- NBER: National Bureau of Economic Research: available at: <http://www.nber.org/cycles/sept2010.html> (last access: September 2010), 2010.
- Newman, S., Xu, X., Affek, H. P., Stolper, E., and Epstein, S.: Changes in mixing ratio and isotopic composition of CO₂ in urban air from the Los Angeles basin, California, between 1972 and 2003, *J. Geophys. Res.-Atmos.*, 113, D23304, doi:10.1029/2008JD009999, 2008.
- Newman, S., Jeong, S., Fischer, M. L., Xu, X., Haman, C. L., Lefer, B., Alvarez, S., Rap-penglueck, B., Kort, E. A., Andrews, A. E., Peischl, J., Gurney, K. R., Miller, C. E., and Yung, Y. L.: Diurnal tracking of anthropogenic CO₂ emissions in the Los Angeles basin megacity during spring 2010, *Atmos. Chem. Phys.*, 13, 4359–4372, doi:10.5194/acp-13-4359-2013, 2013.

CO₂ emissions trends in the Los Angeles megacity

S. Newman et al.

Title Page

Abstract

Introduction

Conclusions

References

Tables

Figures



Back

Close

Full Screen / Esc

Printer-friendly Version

Interactive Discussion



- NRC, National Research Council: Advancing the Science of Climate Change National Research Council. The National Academies Press, Washington, DC, USA, 2010.
- Pataki, D., Bowling, D., and Ehleringer, J.: Seasonal cycle of carbon dioxide and its isotopic composition in an urban atmosphere: anthropogenic and biogenic effects, *J. Geophys. Res.*, 108, 4735, doi:10.1029/2003JD003865, 2003.
- Patarasuk, R., Gurney, K. R., O’Keeffe, D., Song, Y., Huang, J., Rao, P., Buchert, M., Lin, J., Mendoza, D., and Ehleringer, J.: High-resolution fossil fuel CO₂ emissions quantification and application to urban climate policy, *Urban Ecosys.*, in preparation, 2015.
- Peters, G., Marland, G., Le Quéré, C., and Boden, T.: Rapid growth in CO₂ emissions after the 2008–2009 global financial crisis, *Nature Climate Change*, 2, 2–4, 2012.
- Prinn, R. G., Weiss, R. F., Fraser, P. J., Simmonds, P. G., Cunnold, D. M., Alyea, F. N., O’Doherty, S., Salameh, P., Miller, B. R., Huang, J., Wang, R., Hartley, D. E., Harth, C., Steele, L. P., Sturrock, G., Midgley, P. M., and McCulloch, A.: A history of chemically and radiatively important gases in air deduced from ALE/GAGE/AGAGE, *J. Geophys. Res.-Atmos.*, 105, 17751–17792, doi:10.1029/2000JD900141, 2000.
- Rao, P., Gurney, K. R., Patarasuk, R., Song, Y., Miller, C. E., Duren, R. M. Duren, and Elderling, A.: Spatio-temporal variations in onroad vehicle fossil fuel CO₂ emissions in Los Angeles megacity, *Environ. Sci. Technol.*, submitted, 2015.
- Rolph, G. D.: Real-time Environmental Applications and Display sYstem (READY), available at: <http://www.ready.noaa.gov> (last access: July 2015), NOAA Air Resources Laboratory, College Park, MD, 2014.
- Tans, P. P., Berry, J. A., and Keeling, R. F.: Oceanic 13C/12C observations: a new window on ocean CO₂ uptake, *Global Biogeochem. Cy.*, 7, 353–368, doi:10.1029/93GB00053, 1993.
- Thoning, K., Tans, P., and Komhyr, W.: Atmospheric carbon dioxide at Mauna Loa Observatory, 2, Analysis of the NOAA/GMCC data, 1974–1985, *J. Geophys. Res.*, 94, 8549–8565, 1989.
- Turnbull, J., Miller, J., Lehman, S., Tans, P., Sparks, R., and Southon, J.: Comparison of ¹⁴CO₂, CO, and SF₆ as tracers for recently added fossil fuel CO₂ in the atmosphere and implications for biological CO₂ exchange, *Geophys. Res. Lett.*, 33, L01817, doi:10.1029/2005GL024213, 2006.
- Turnbull, J., Rayner, P., Miller, J., Naegler, T., Ciais, P., and Cozic, A.: On the use of (CO₂)-C-14 as a tracer for fossil fuel CO₂: quantifying uncertainties using an atmospheric transport model, *J. Geophys. Res.-Atmos.*, 114, D22302, doi:10.1029/2009JD012308, 2009.

CO₂ emissions trends in the Los Angeles megacity

S. Newman et al.

Title Page

Abstract

Introduction

Conclusions

References

Tables

Figures



Back

Close

Full Screen / Esc

Printer-friendly Version

Interactive Discussion



- Turnbull, J. C., Karion, A., Fischer, M. L., Faloona, I., Guilderson, T., Lehman, S. J., Miller, B. R., Miller, J. B., Montzka, S., Sherwood, T., Saripalli, S., Sweeney, C., and Tans, P. P.: Assessment of fossil fuel carbon dioxide and other anthropogenic trace gas emissions from airborne measurements over Sacramento, California in spring 2009, *Atmos. Chem. Phys.*, 11, 705–721, doi:10.5194/acp-11-705-2011, 2011.
- Turnbull, J. C., Sweeney, C., Karion, A., Newberger, T., Lehman, S. J., Tans, P. P., Davis, K. J., Lauvaux, T., Miles, N. L., Richardson, S. J., Cambaliza, M. O., Shepson, P. B., Gurney, K., Patarasuk, R., and Razlivanov, I.: Toward quantification and source sector identification of fossil fuel CO₂ emissions from an urban area: results from the INFLUX experiment, *J. Geophys. Res.-Atmos.*, 120, 292–312, doi:10.1002/2014JD022555, 2015.
- Vardag, S. N., Gerbig, C., Janssens-Maenhout, G., and Levin, I.: Estimation of continuous anthropogenic CO₂ using CO₂, CO, $\delta^{13}\text{C}(\text{CO}_2)$ and $\Delta^{14}\text{C}(\text{CO}_2)$, *Atmos. Chem. Phys. Discuss.*, 15, 20181–20243, doi:10.5194/acpd-15-20181-2015, 2015.
- Widory, D. and Javoy, M.: The carbon isotope composition of atmospheric CO₂ in Paris, *Earth Planet. Sc. Lett.*, 215, 289–298, 2003.
- Wong, K. W., Fu, D., Pongetti, T. J., Newman, S., Kort, E. A., Duren, R., Hsu, Y.-K., Miller, C. E., Yung, Y. L., and Sander, S. P.: Mapping CH₄: CO₂ ratios in Los Angeles with CLARS-FTS from Mount Wilson, California, *Atmos. Chem. Phys.*, 15, 241–252, doi:10.5194/acp-15-241-2015, 2015.
- World Bank: GDP, <http://data.worldbank.org/indicator/NY.GDP.MKTP.CD/countries/1W-US?display=graph>, last access: May 2015.
- Wu, Z. and Huang, N. E.: Ensemble empirical mode decomposition: a noise-assisted data analysis method, *Adv. Adapt. Data. Anal.*, 1, 1–41, 2009.
- Xu, X., Trumbore, S. E., Zheng, S., Southon, J. R., McDuffee, K. E., Luttgen, M., and Liu, J. C.: Modifying a sealed tube zinc reduction method for preparation of AMS graphite targets: reducing background and attaining high precision, *Nucl. Instrum. Meth. B*, 259, 320–329, 2007.
- York, R.: Asymmetric effects of economic growth and decline on CO₂ emissions, *Nature Climate Change*, 2, 762–764, doi:10.1038/nclimate1699, 2012.

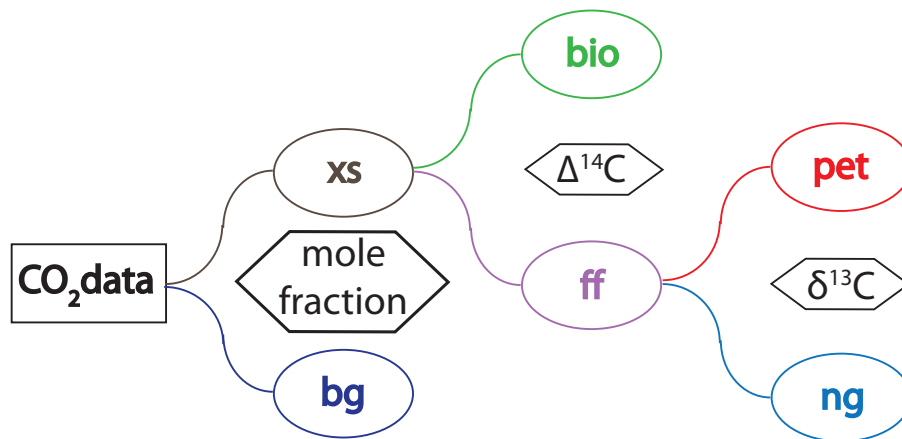


Figure 2. Schematic diagram showing the use of different data sets for attribution of the sources of CO₂ emissions. Mole fractions of background (bg) and observations are used to determine C_{xs} (excess over background/bg); $\Delta^{14}\text{C}$ values are used to distinguish C_{ff} (fossil fuel, ff) and C_{bio} (biosphere, bio); $\delta^{13}\text{C}$ compositions are used to distinguish C_{pet} (petroleum/gasoline, pet) from C_{ng} (natural gas, ng).

CO₂ emissions trends in the Los Angeles megacity

S. Newman et al.

Title Page	
Abstract	Introduction
Conclusions	References
Tables	Figures
◀	▶
◀	▶
Back	Close
Full Screen / Esc	
Printer-friendly Version	
Interactive Discussion	



CO₂ emissions trends in the Los Angeles megacity

S. Newman et al.

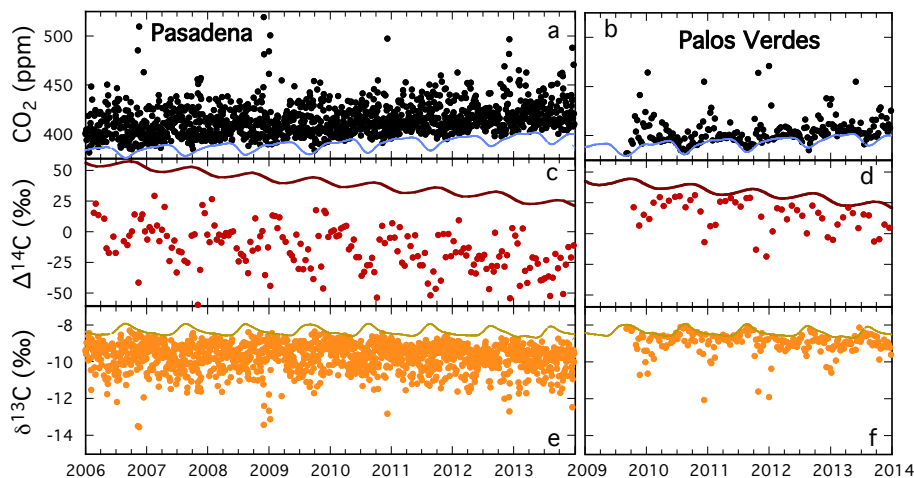


Figure 3. Time series of CO₂ mole fractions for ¹⁴CO₂ samples (a, b), Δ¹⁴C data (c, d), and δ¹³C (e, f) for Pasadena and Palos Verdes. The solid curves are backgrounds used in the calculations: δ¹³C and CO₂ backgrounds are from La Jolla, CA and Δ¹⁴C from Pt. Barrow, AK.

[Title Page](#)[Abstract](#)[Introduction](#)[Conclusions](#)[References](#)[Tables](#)[Figures](#)[Back](#)[Close](#)[Full Screen / Esc](#)[Printer-friendly Version](#)[Interactive Discussion](#)

CO₂ emissions trends in the Los Angeles megacity

S. Newman et al.

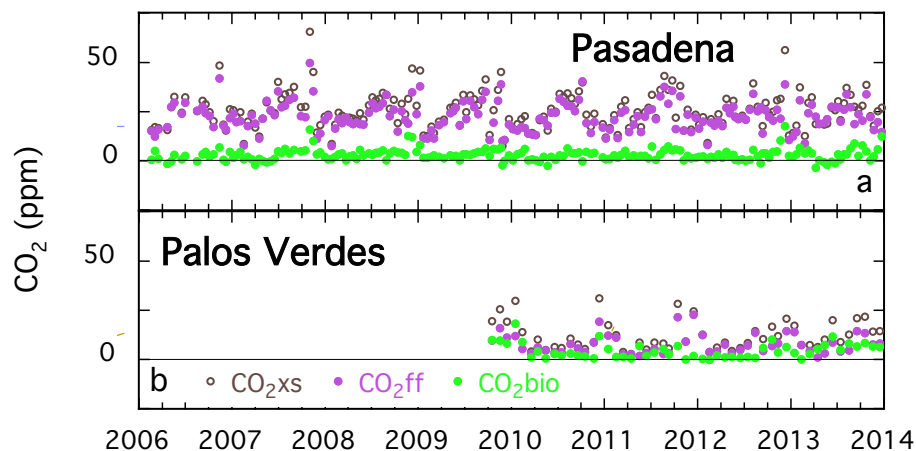


Figure 4. Time series of C_{XS} , C_{ff} , and C_{bio} calculated from $\Delta^{14}\text{C}$ (see text for description of calculations) for Pasadena (top) and Palos Verdes (bottom). The errors for C_{ff} are 1 ppm. The negative C_{bio} values indicate photosynthetic uptake. The value of $\Delta^{14}\text{C}$ for fuel for this calculation was taken to be -954‰ , the average from the summer and winter calculations.

Title Page

Abstract

Introduction

Conclusions

References

Tables

Figures



Back

Close

Full Screen / Esc

Printer-friendly Version

Interactive Discussion



CO₂ emissions trends in the Los Angeles megacity

S. Newman et al.

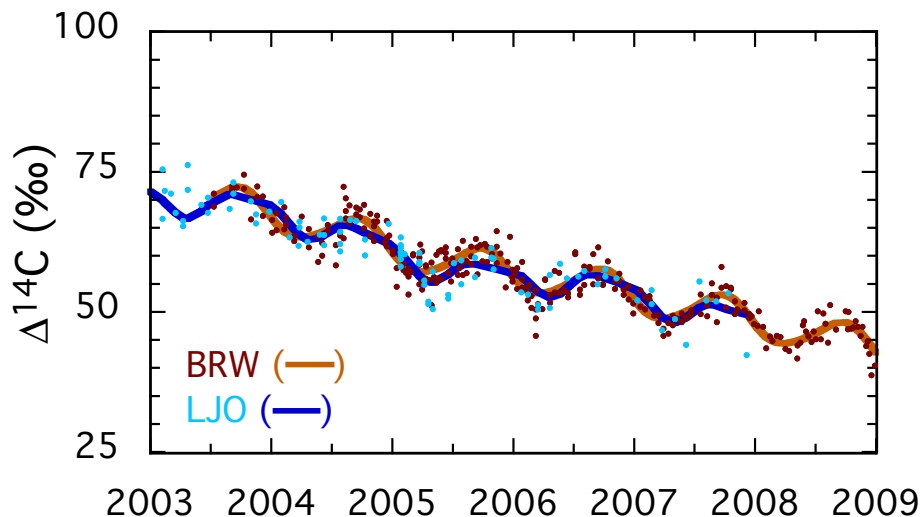


Figure 5. Comparison of possible background records for this study, Pt. Barrow, AK, (BRW; Xiaomei Xu, unpublished data) and La Jolla, CA (LJO; Graven et al., 2012). The smoothed brown curve for BRW is the $\Delta^{14}\text{C}$ background used for this study and was calculated using the algorithm of Thoning et al. (1989), from the function plus the smoothed residuals of the long-term trend, using 2 harmonic and 3 polynomial terms in the function and 667 days as the long-term cutoff for the low-pass filter.

[Title Page](#)[Abstract](#)[Introduction](#)[Conclusions](#)[References](#)[Tables](#)[Figures](#)[◀](#)[▶](#)[◀](#)[▶](#)[Back](#)[Close](#)[Full Screen / Esc](#)[Printer-friendly Version](#)[Interactive Discussion](#)

CO₂ emissions trends in the Los Angeles megacity

S. Newman et al.

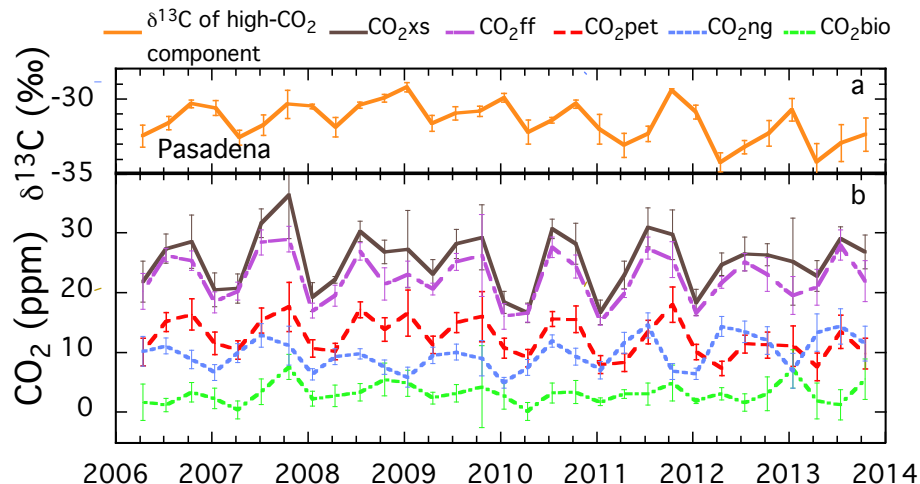


Figure 6. Attribution of CO₂ excess in Pasadena among combustion of natural gas and petroleum and the biosphere. **(a)** Miller–Tans slopes for seasonal averages of monthly plots. Error bars are standard errors of the regression intercepts. **(b)** Attribution of C_{xs} among all three sources (natural gas, petroleum, and the biosphere), combining the information from Δ¹⁴C and δ¹³C, using Miller–Tans slopes to determine the relative proportions of petroleum and natural gas combustion. Error bars are propagated from the errors in the δ¹³C intercepts and the Δ¹⁴C measurements.

Title Page	
Abstract	Introduction
Conclusions	References
Tables	Figures
◀	▶
◀	▶
Back	Close
Full Screen / Esc	
Printer-friendly Version	
Interactive Discussion	



CO₂ emissions trends in the Los Angeles megacity

S. Newman et al.

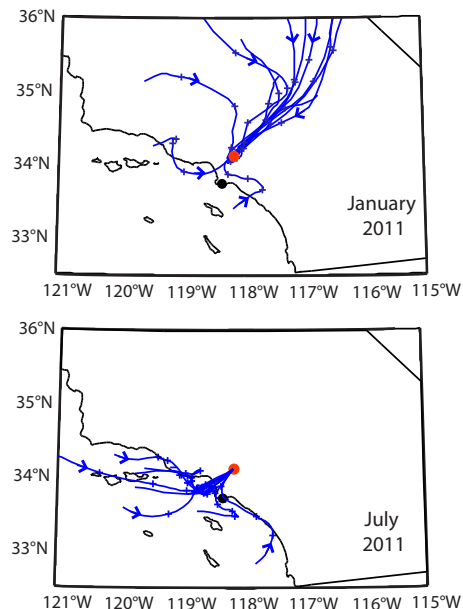


Figure 7. Back trajectories (24 h) for winds arriving at the Pasadena site (red dot) at 14:00 PST for January **(a)** and July **(b)** 2011, calculated by HYSPLIT (Draxler and Rolph, 2015) for all sampling days in January and selected sampling days in July, for clarity. Results for all sampling days are shown in Fig. A2. Arrows indicate the direction of air flow. Plus signs indicate 6, 12, and 18 h from the Pasadena site. The black dot is the location of the Palos Verdes site. The back trajectories for the Palos Verdes site show a similar pattern (Appendix Fig. A2). The back trajectories explain the difference between the annual cycles at the two sites, shown in Fig. 8.

Title Page	
Abstract	Introduction
Conclusions	References
Tables	Figures
◀	▶
◀	▶
Back	Close
Full Screen / Esc	
Printer-friendly Version	
Interactive Discussion	



**CO₂ emissions
trends in the Los
Angeles megacity**

S. Newman et al.

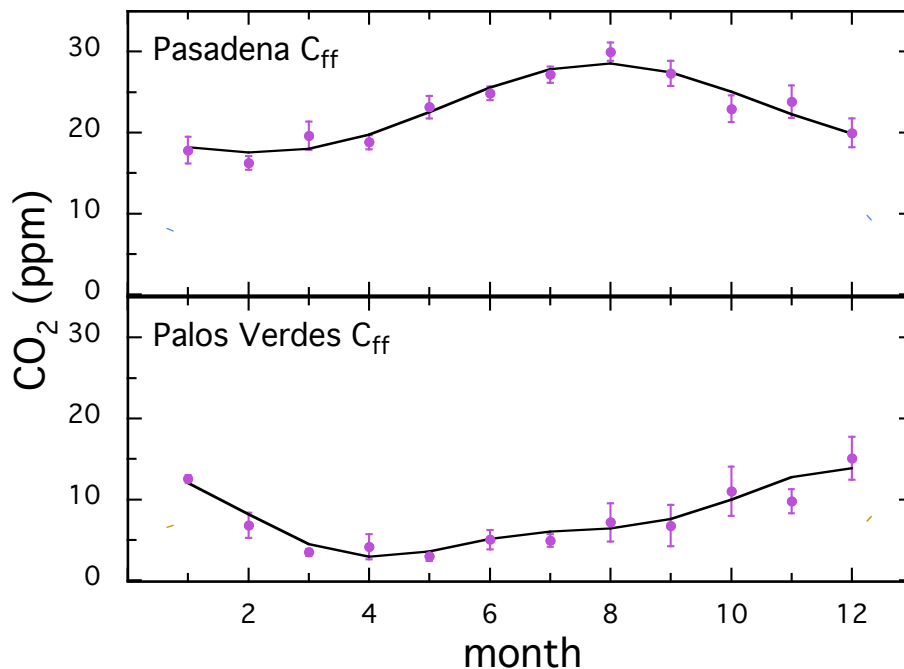


Figure 8. The annual patterns for C_{ff} in Pasadena and Palos Verdes calculated as the best fit of two harmonics plus the average of the annual cycles (black curves). These patterns are consistent with seasonal differences in the back trajectories shown in Fig. 7.

[Title Page](#)[Abstract](#)[Introduction](#)[Conclusions](#)[References](#)[Tables](#)[Figures](#)[◀](#)[▶](#)[◀](#)[▶](#)[Back](#)[Close](#)[Full Screen / Esc](#)[Printer-friendly Version](#)[Interactive Discussion](#)

CO₂ emissions trends in the Los Angeles megacity

S. Newman et al.

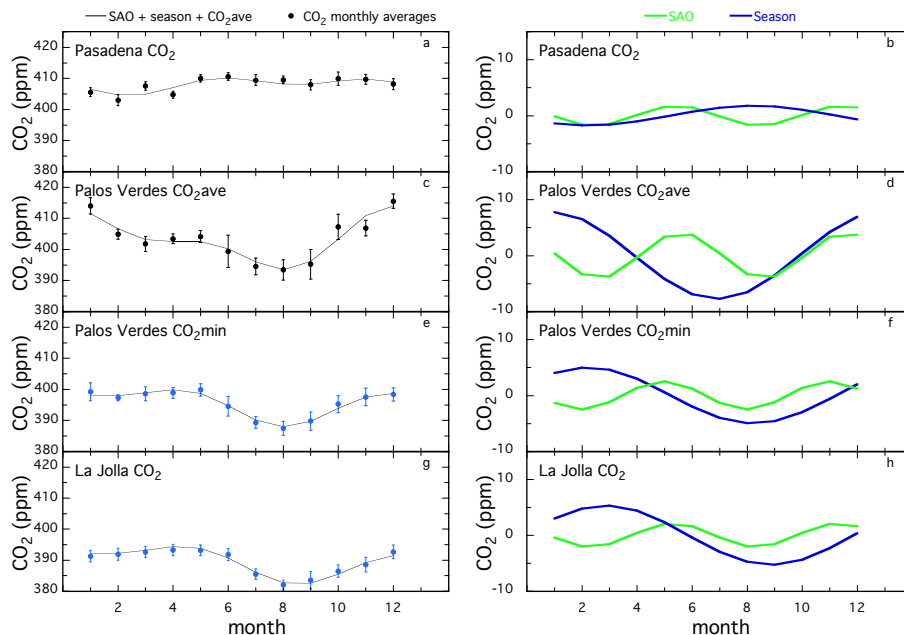


Figure 9. Comparison of seasonal and semi-annual oscillation cycles of CO₂ mole fractions for flask samples from Pasadena (2006–2013) with those at the La Jolla (2006–2013) and Palos Verdes (2009–2013) sites. Left column panels show the average annual patterns for the monthly averages together with the sum of the harmonics for seasonal (blue) and semi-annual (green) cycles (Jiang et al., 2008). Right column panels show the amplitudes and phases of the pure harmonic components. Two sets of results are shown for Palos Verdes, for the monthly averages (**c**, **d**) and for the monthly averages of weekly minima (**e**, **f**). The monthly averages show the effect of transport on the signal, with a large peak during the winter, while the minima (in blue) show that data from this site are very similar to La Jolla (in blue) and should be a good estimation of the background air for the LA basin. Error bars on the monthly averages of the data are 1σ standard errors.

Title Page

Abstract Introduction

Conclusions References

Tables Figures

◀ ▶

◀ ▶

Back Close

Full Screen / Esc

Printer-friendly Version

Interactive Discussion



CO₂ emissions trends in the Los Angeles megacity

S. Newman et al.

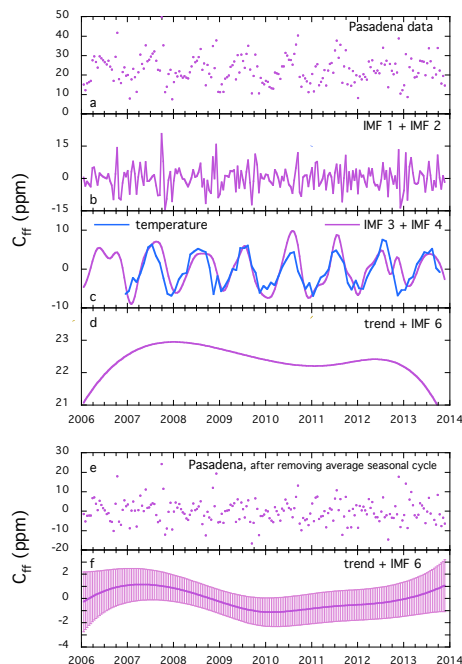


Figure 10. Results of ensemble empirical mode decomposition (EEMD) (Huang et al., 1998; Wu and Huang, 2009) of the C_{ff} time series calculated using Eq. (3) and the average, constant $\Delta^{14}\text{C}$ of -954‰ for fossil fuel. The top set of panels show the raw data (**a**), noise (**b**), annual and semi-annual mode (**c**), and the trend + IMF 6 (**d**). The pattern of the trend + IMF 6 shown in (**d**) is within 1σ uncertainty of no variation over this time period. The bottom two panels include the raw data after subtracting the average annual cycle (**e**), and the trend + IMF 6 for the modified data set (**f**). 30 day average temperatures (minus the overall average and scaled to match the magnitude of the C_{ff} IMF; blue curve) are superimposed on the plot of IMF 3 + IMF 4 (**c**). Shaded regions in (**f**) indicate 1σ standard deviation of 300 Monte Carlo realizations with 13.7 % noise added, the ratio of the uncertainty in C_{ff} to the standard deviation of the data.

[Title Page](#)
[Abstract](#)
[Introduction](#)
[Conclusions](#)
[References](#)
[Tables](#)
[Figures](#)

[Back](#)
[Close](#)
[Full Screen / Esc](#)
[Printer-friendly Version](#)
[Interactive Discussion](#)


CO₂ emissions trends in the Los Angeles megacity

S. Newman et al.

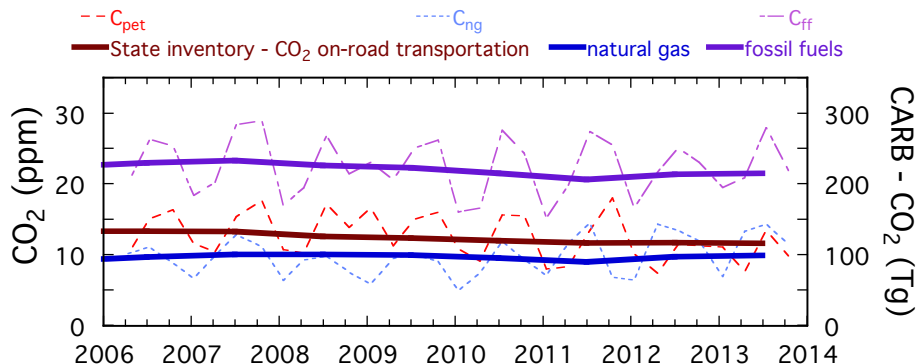


Figure 11. Comparison of annual average CO₂ emissions from bottom-up California Air Resources Board (CARB) inventories (thick lines; right axis labels) for fossil fuel-derived emissions with top-down seasonal averages from the Pasadena data, using the Miller and Tans (2003) approach to attribute CO₂ emissions from petroleum and natural gas combustion from the $\delta^{13}\text{C}$ measurements. Seasonal curves showing the attribution of C_{xs} from Fig. 6b are shown as thin lines. The annual trends from the bottom-up CARB inventories are plotted on a scale exactly 100 times that of the trends derived from the CO₂ measurements, showing that the relative proportions are very similar through 2013.

Title Page

Abstract

Introduction

Conclusions

References

Tables

Figures



Back

Close

Full Screen / Esc

Printer-friendly Version

Interactive Discussion



CO₂ emissions trends in the Los Angeles megacity

S. Newman et al.

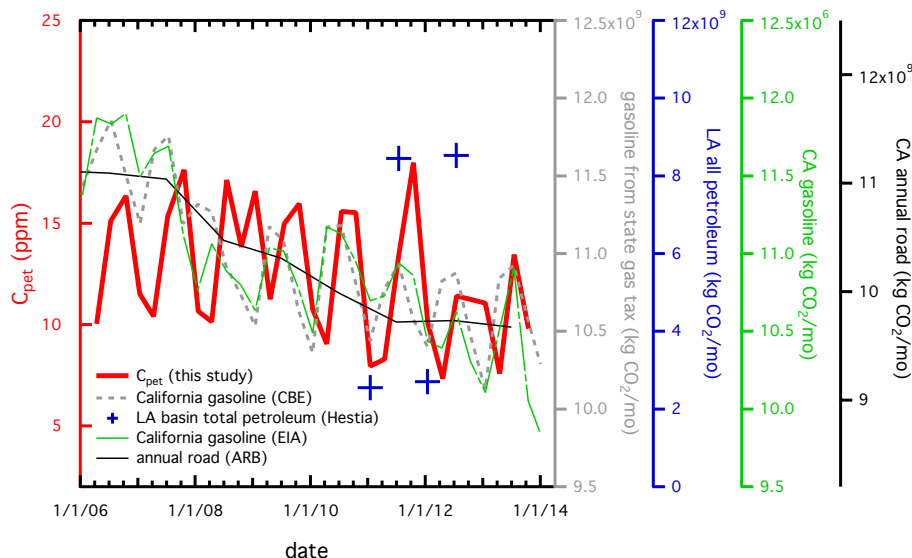


Figure 12. Comparison of the Pasadena C_{pet} atmospheric concentration with all available area-integrated bottom-up fossil fuel CO₂ emissions, including gasoline sales based on taxes paid to the California Board of Equalization (CBE, 2014), gasoline provided in California by prime suppliers, the California Air Resources Board’s annual road emissions (CARB, 2015), and the Hestia-LA gridded total petroleum. The Hestia-LA data product is specific to the Los Angeles megacity domain; all inventories are statewide estimates. Since the Hestia-LA product is gridded, we show the emissions emanating from different regions for January (northeast quadrant, Fig. 13a) and July (southwest quadrant), based on prevailing winds during those periods (Figs. 7 and 13a). The axis for each inventory has been adjusted to allow easy comparison. The seasonality of the C_{pet} data lags the bottom-up inventories by a few months. This analysis is consistent with the observed decrease in gasoline combustion during 2008–2011.

Title Page	
Abstract	Introduction
Conclusions	References
Tables	Figures
◀	▶
◀	▶
Back	Close
Full Screen / Esc	
Printer-friendly Version	
Interactive Discussion	



CO₂ emissions trends in the Los Angeles megacity

S. Newman et al.

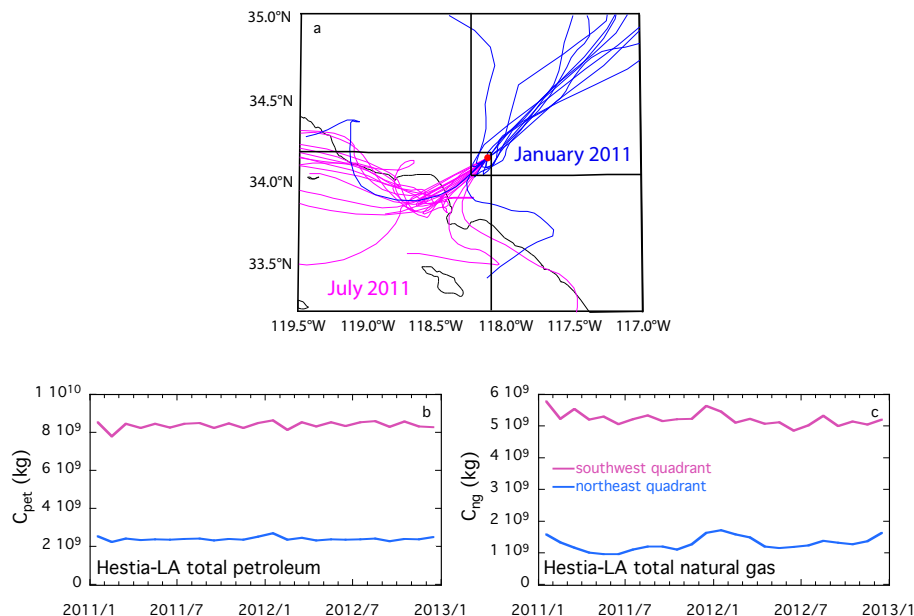


Figure 13. Relevant emissions selection from the Hestia-LA data product. **(a)** Quadrants selected for investigation of CO₂ emissions from the Hestia-LA data product, together with the 24 h back trajectories calculated by HYSPLIT for January (northeast quadrant) and July (southwest quadrant) $\Delta^{14}\text{C}$ sampling days. The back trajectories end in Pasadena (red dot) at 14:00 PST. Monthly averaged time series for Hestia-LA data product C_{ff} are shown from total petroleum combustion **(b)** and total natural gas combustion **(c)** for 2011 and 2012. For both the northeast quadrant of the Los Angeles region, the source of winter emissions, and the southwest quadrant, the source of summer emissions, the seasonal pattern is either flat (petroleum) or characterized by peaks during the winter (natural gas). But the summer emissions are always higher than those during winter, consistent with the observed top-down patterns for C_{pet} and C_{ng} in Pasadena.

CO₂ emissions trends in the Los Angeles megacity

S. Newman et al.

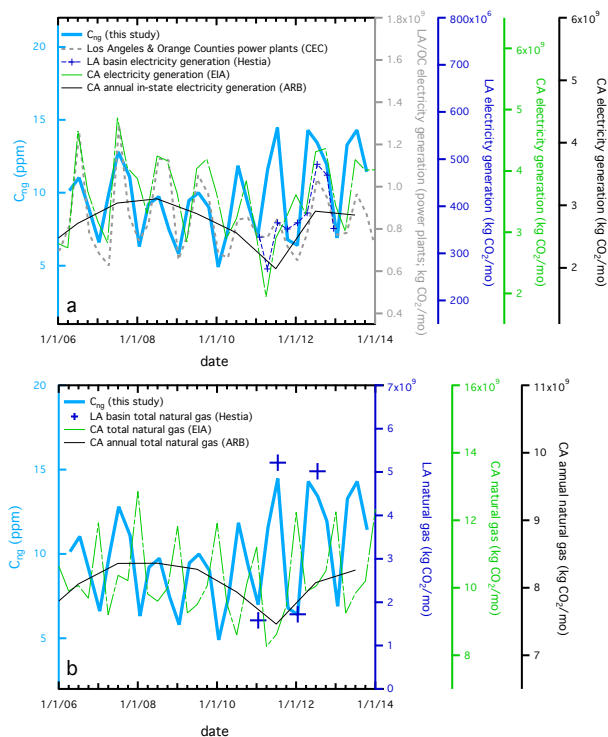


Figure 14. Comparison of Pasadena C_{ng} atmospheric concentration with area-integrated inventories of natural gas combustion, as well as the gridded Hestia-LA data product for southwest and northeast regional sectors for July and January months, respectively. Panel (a) compares the data from this paper with usage of natural gas by the electrical power sector; panel (b) shows the comparison with total natural gas consumption. Statewide inventories are given by EIA (2014) and CARB (2015) curves. Regional inventories include Hestia results and natural gas from power plants (CEC, 2014) in Los Angeles and Orange counties with monthly data (except Calabasas and Valencia). The vertical axes have been adjusted to allow easy comparison. This analysis is consistent with the increase in natural gas usage during the last few years.

CO₂ emissions trends in the Los Angeles megacity

S. Newman et al.

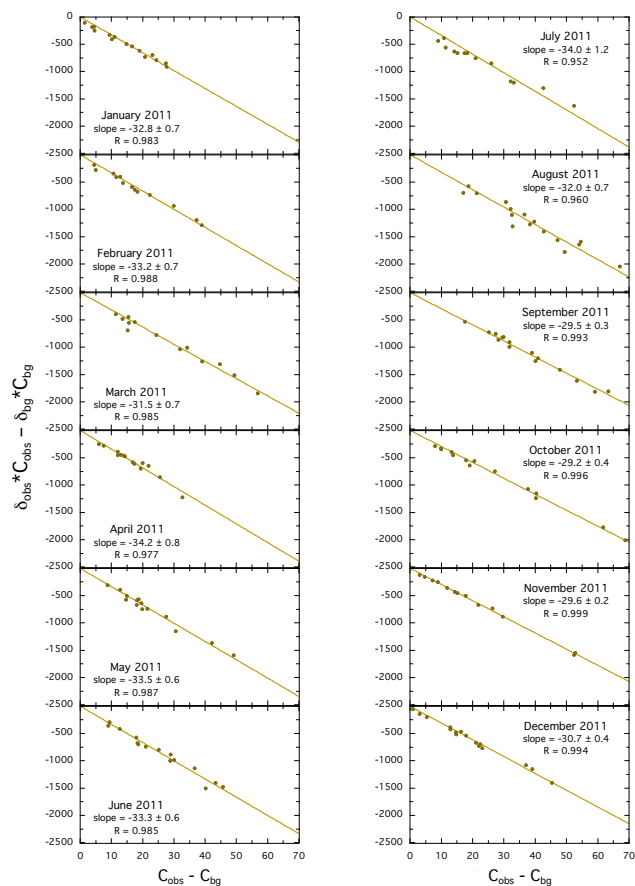


Figure A1. Miller-Tans plots for each month in 2011. Values of the slopes for three-month seasonal averages are plotted in Fig. 6a.

Title Page

Abstract

Introduction

Conclusions

References

Tables

Figures



Back

Close

Full Screen / Esc

Printer-friendly Version

Interactive Discussion



**CO₂ emissions
trends in the Los
Angeles megacity**

S. Newman et al.

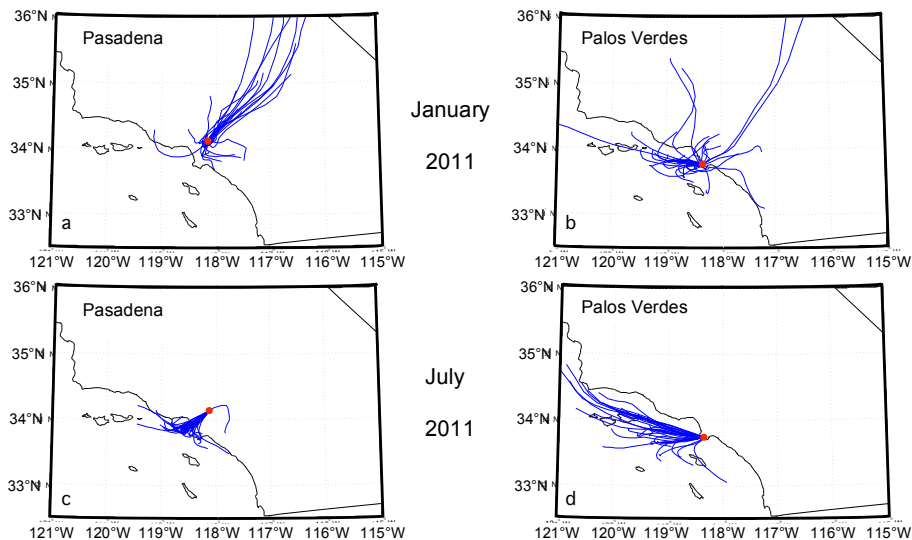


Figure A2. Twelve-hour back trajectories for all days in January and July 2011, for the Pasadena and Palos Verdes sites. This shows more detail for the effect of transport on the air masses sampled during summer and winter at the Palos Verdes site than Fig. 7.

[Title Page](#)[Abstract](#)[Introduction](#)[Conclusions](#)[References](#)[Tables](#)[Figures](#)[Back](#)[Close](#)[Full Screen / Esc](#)[Printer-friendly Version](#)[Interactive Discussion](#)

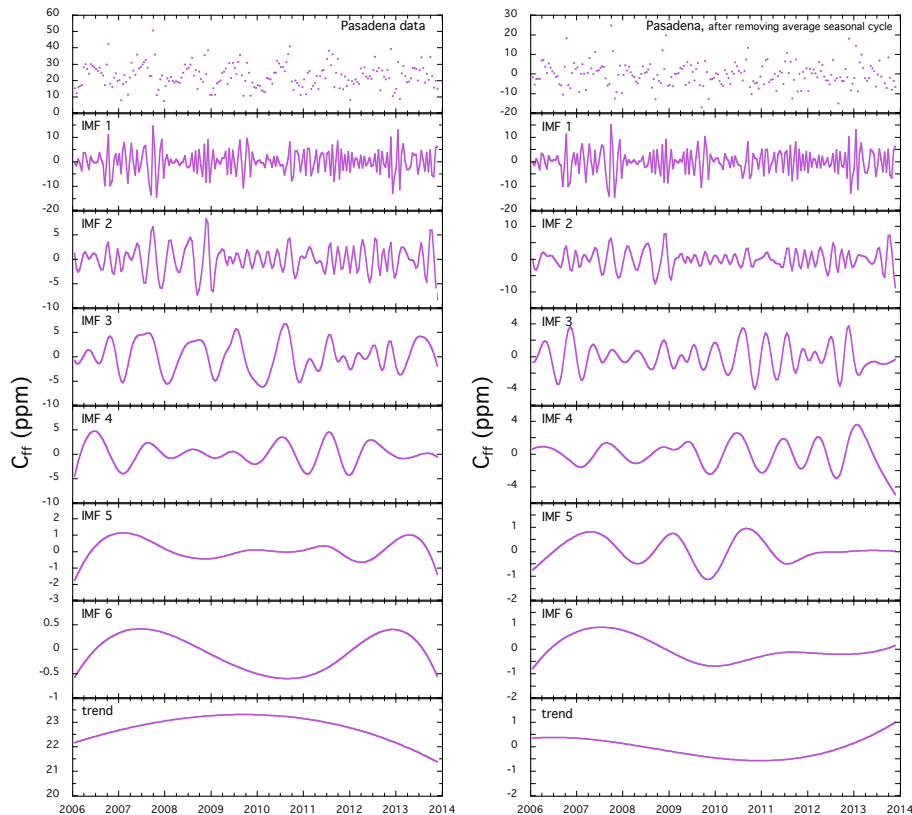


Figure A3. Time series of all of the results from the ensemble empirical mode decomposition (EEMD) analysis of the Pasadena C_{ff} . The left set of panels shows the results for the raw data, whereas the right column shows those for the data after subtraction of the average seasonal cycle. The long-term trend reflecting the economic downturn of the Great Recession is reflected clearly in IMF 6 and the trend of the data after the pronounced seasonality is removed (right-hand column), although there is some evidence of it in IMF 6 of the raw C_{ff} data.

CO₂ emissions trends in the Los Angeles megacity

S. Newman et al.

Title Page

Abstract

Introduction

Conclusions

References

Tables

Figures

◀

▶

◀

▶

Back

Close

Full Screen / Esc

Printer-friendly Version

Interactive Discussion

